JACS
JOURNAL OF THE AMERICAN CHEMICAL SOCIETY
Article
pubs.acs.org/JACS

Large-Scale Production of Edge-Selectively Functionalized Graphene Nanoplatelets via Ball Milling and Their Use as Metal-Free Electrocatalysts for Oxygen Reduction Reaction

In-Yup Jeon,[†,§] Hyun-Jung Choi,[†,§] Sun-Min Jung,[†] Jeong-Min Seo,[†] Min-Jung Kim,[†] Liming Dai,[†,‡] and Jong-Beom Baek*[,†]

[†]Ulsan National Institute of Science and Technology (UNIST), Interdisciplinary School of Green Energy/Low-Dimensional Carbon Materials Center, 100 Banyeon, Ulsan 689-897, South Korea

[‡]Department of Macromolecular Science and Engineering, Case Western Reserve University, 10900 Euclid Avenue, Cleveland, Ohio 44106, United States

Supporting Information

ABSTRACT: Edge-selectively functionalized graphene nanoplatelets (EFGnPs) with different functional groups were efficiently prepared simply by dry ball milling graphite in the presence of hydrogen, carbon dioxide, sulfur trioxide, or carbon dioxide/sulfur trioxide mixture. Upon exposure to air moisture, the resultant hydrogen- (HGnP), carboxylic acid- (CGnP), sulfonic acid- (SGnP), and carboxylic acid/sulfonic acid- (CSGnP) functionalized GnPs readily dispersed into various polar solvents, including neutral water. The resultant EFGnPs were then used as electrocatalysts for oxygen reduction reaction (ORR) in an alkaline electrolyte. It was found that the edge polar nature of the newly prepared EFGnPs without heteroatom doping into their basal plane played an important role in regulating the ORR efficiency with the electrocatalytic activity in the order of SGnP > CSGnP > CGnP > HGnP > pristine graphite. More importantly, the sulfur-containing SGnP and CSGnP were found to have a superior ORR performance to commercially available platinum-based electrocatalyst.

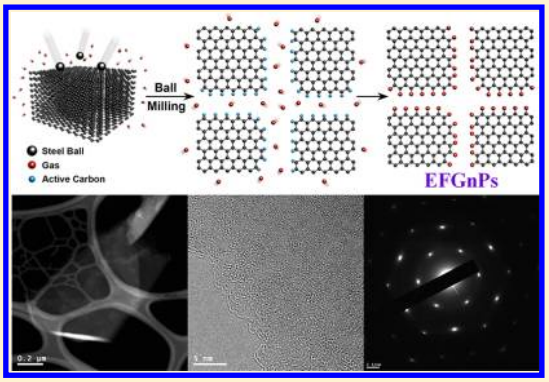

INTRODUCTION

The electrocatalytic activity of heteroatom-doped carbon-based nanomaterials has become a growing interest in the past few years due to their potential applications for fuel cells[1] and metal−air batteries.[2] Several approaches, including chemical vapor deposition (CVD),[3] the chemical derivatization of graphite oxide (GO),[4−6] and edge-functionalization of graphite (EFG),[7] have been exploited for the doping of heteroatoms, such as nitrogen and boron, or both, into graphitic structures. Although the CVD method led to the initial discovery of nitrogen-doped CNTs (N-CNTs)[8] and graphene (N-graphene)[3] as metal-free electrocatalysts for oxygen reduction reaction (ORR), this approach is undesirable for the scalable production of heteroatom-doped carbon nanomaterials due to costs and technical challenges. The recent availability of solution-processable GO by physicochemical exfoliation, followed by solution reduction[9−11] and/or heat-treatment[12] in the presence of appropriate chemical reagent(s) (e.g., ammonia) has allowed for the mass production of nitrogen-doped graphene nanoplatelets (NGnP) via an all-solution process. However, the solution exfoliation of graphite into GO involves strong, hazardous oxidizing reagents (e.g., HNO_3 and/or H_2SO_4)[13] and a tedious multistep process.[9,14] Such a corrosive chemical oxidation often leads to severe damage of the graphitic basal plane by introducing a large number of chemical and topological defects[15] to cause detrimental effects on the electron transfer and structural integrity. As a result, the postexfoliation reduction of GO into a reduced graphene oxide (rGO) is essential in order to restore the graphitic structure within the resultant GnPs.[16,17] Unfortunately, the reduction reaction also involves hazardous (carcinogenic) reducing reagents (e.g., hydrazine, $NaBH_4$). Due to an inherently low reduction conversion (~70%) limited by edge reduction and subsequent edge-zipping to hamper the basal area reduction, the resultant rGO still contains considerable chemical and structural defects.[18] Nevertheless, the GO to rGO process has so far been considered to be one of the most reliable methods for the mass production of graphene, though it still remains elusive. Recently, we have developed an alternative approach to the large-scale production of edge-carboxylated GnPs (CGnP) without basal plane distortion via simple and ecofriendly ball milling of graphite in the presence of dry ice (solid state of carbon dioxide).[19] Furthermore, we have also demonstrated that the electrocatalytic activity of carbon nanotubes without

Received: September 15, 2012
Published: October 30, 2012

dx.doi.org/10.1021/ja3091643 | J. Am. Chem. Soc. 2013, 135, 1386−1393

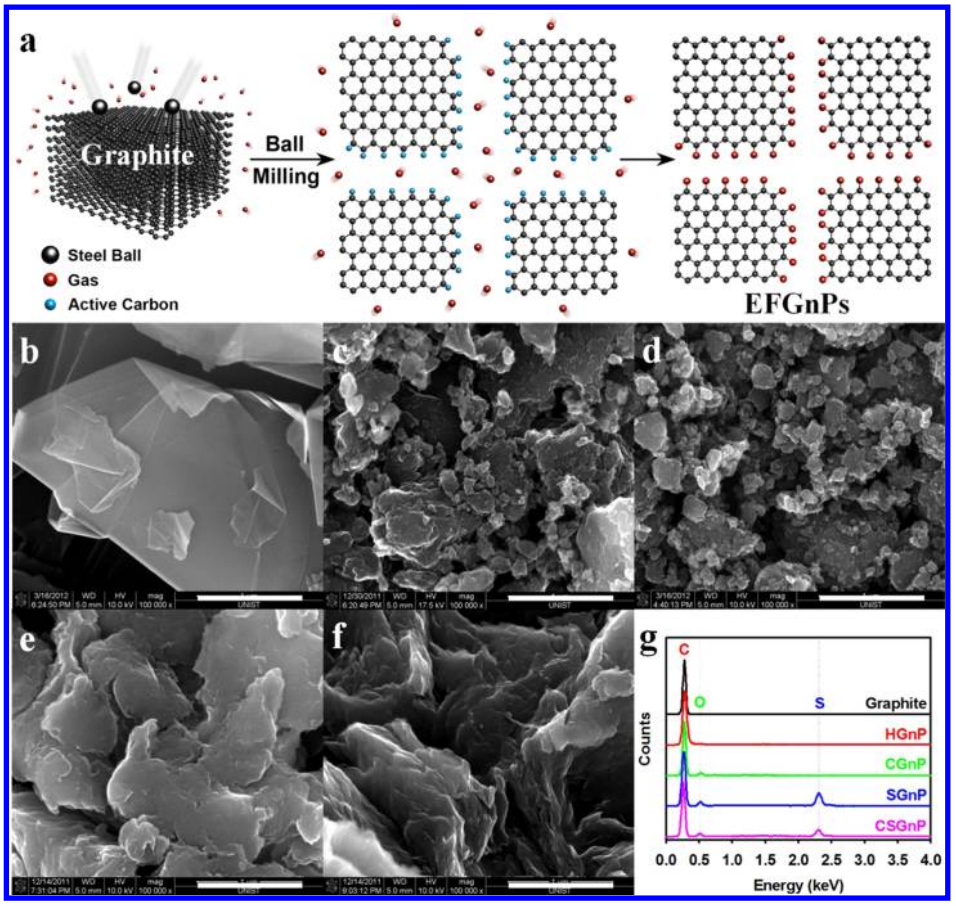

Figure 1. (a) Schematic representation of the mechanochemical reaction between in situ generated active carbon species and reactant gases in a sealed ball-mill crusher. The cracking of graphite by ball milling in the presence of corresponding gases and subsequent exposure to air moisture resulted in the formation of EFGnPs. The red balls stand for reactant gases such as hydrogen, carbon dioxide, sulfur trioxide, and air moisture (oxygen and moisture). SEM images: (b) the pristine graphite; (c) HGnP; (d) CGnP; (e) SGnP; (f) CSGnP. Scale bars are 1 μm. (g) EDX spectra of the pristine graphite and EFGnPs.

heteroatom doping is significantly affected by its periphery polarity.[20]

On the basis of our new fundamental findings,[21,22] we prepared in this study a series of edge-selectively functionalized GnPs (EFGnPs) with different edge groups and minimal basal plane distortion by simply dry ball milling graphite in the presence of various gases or gas mixture(s). The resultant EFGnPs are highly dispersible in various polar solvents, leading to a large-scale production of EFGnPs. The electrocatalytic activities of these EFGnPs without heteroatom-doping on their basal planes were investigated for an ORR in an alkaline electrolyte. Possible effects of the edge nature (polarity) of EFGnPs on the ORR electrocatalytic activity in an alkaline electrolyte were evaluated in terms of both the thermodynamic (oxygen physisorption on electrodes) and kinetic (oxygen diffusion to electrodes) aspects.[8]

■ RESULTS AND DISCUSSION

Due to the versatility of mechanochemical reactions driven by ball milling, various functional groups could be introduced at the broken edges of graphite in the presence of appropriate chemical vapors, liquids, or solids in the ball-mill crusher.[21] Thus, the methodology used in this study is a low-cost, high-yield, versatile approach to the mass production of GnPs with various desired functional groups.[21] In this work, a series of EFGnPs were prepared by ball milling the graphite (100 mesh, <150 μm) in the presence of hydrogen, dry ice, sulfur trioxide, or a dry ice/sulfur trioxide mixture to produce a large amount (typically 5.0 g for each batch) of hydrogen- (HGnP), carboxylic acid- (CGnP), sulfonic acid (SGnP), and carboxylic acid/sulfonic acid-functionalized (CSGnP) GnPs, respectively (see experimental details in Supporting Information, SI) (Figure 1a). The mechanism of edge-selective functionalization in the ball-milling process involves the reaction between reactive carbon species (radicals and ions) generated by a mechanochemical cleavage of graphitic C−C bonds and gases introduced into a sealed ball-mill crusher (Figure 1a and detailed mechanism in Figure S1). The dormant active carbon species unreacted in the crusher could be terminated by subsequent exposure to air moisture. As a result, some oxygenated groups, such as hydroxyl (−OH) and carboxylic acid (−COOH), could be introduced at the broken edges of the preformed EFGnPs (see Figure S1).

We used a scanning electron microscope (SEM) to demonstrate the mechanochemical cracking of a large grain size of graphite into a small grain size of EFGnPs, as schematically shown in Figure 1a. A typical SEM image of the pristine graphite has a grain size in the range of a few to a hundred micrometers (Figure 1b). After ball milling for 48h, the resultant EFGnPs show dramatically reduced grain sizes in the range of 0.1−1 μm (Figures 1c−f), indicating an obvious size reduction by mechanochemical cracking. Due to the

dx.doi.org/10.1021/ja3091643 | J. Am. Chem. Soc. 2013, 135, 1386−1393

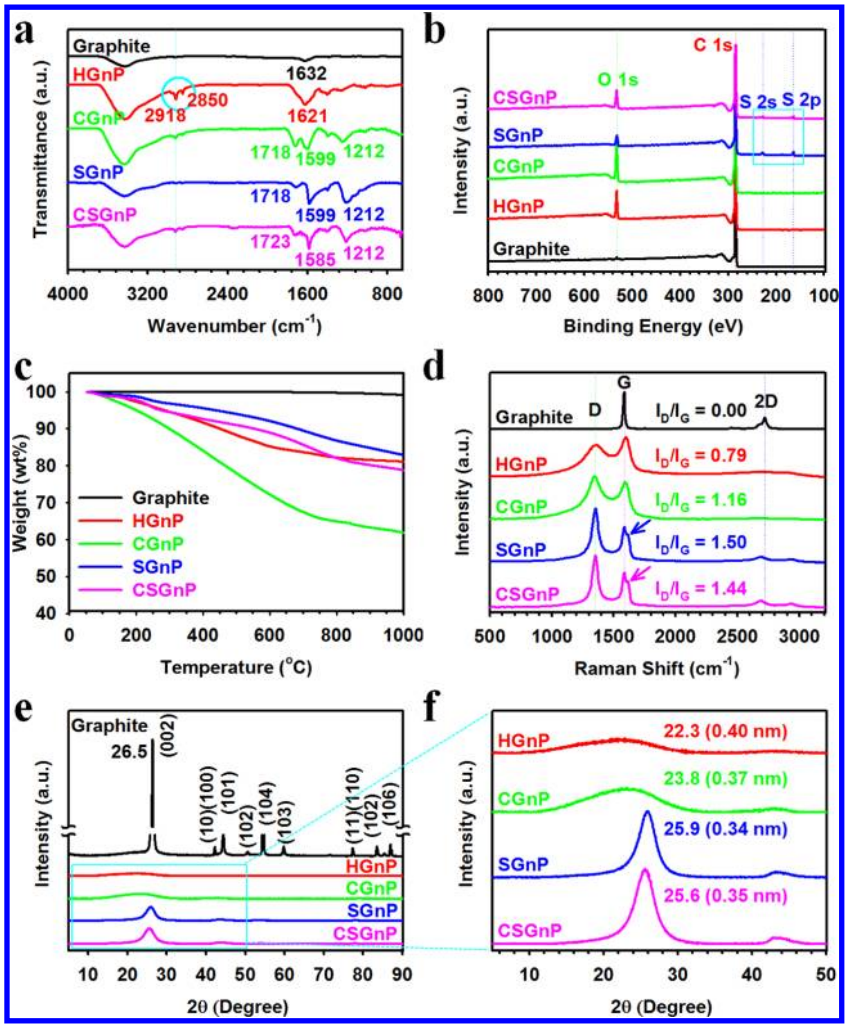

Figure 2. (a) FTIR spectra (KBr pellets); (b) XPS survey spectra; (c) TGA thermograms obtained from the heating rate of 10 °C/min in nitrogen; (d) Raman spectra; (e) XRD diffraction patterns; and (f) magnified XRD diffraction patterns from sky blue rectangle box in (e).

reaction between the newly formed active carbon species at the broken edges of the GnPs and corresponding gases, the ball milling and subsequent workup procedures were found to increase the weight of all the resultant EFGnPs with respect to the graphite starting material (see Experimental Section). These results indicated that the mechanochemical functionalization of graphite was efficient. Interestingly enough, the SEM images in Figure 1 show a more aggregate morphology for the SGnP and CSGnP (Figure 1e,f, respectively) containing polar sulfonic acid groups than the EFGnPs of relatively less polar groups, such as HGnP and CGnP (Figure 1c,d, respectively). The observed difference is presumably due to the formation of strong edge hydrogen bonds for the former, which will be discussed later. As expected, the corresponding energy-dispersive X-ray (EDX) surveys (Figure 1g) and element mappings in Figures S2 and S3 show the presence of constituent elements for each of the samples with sulfur being observed only in SGnP and CSGnP (Figure S3).

The TEM images with selected area electron diffraction (SAED) patterns presented in Figures S4–S7 clearly show the presence of EFGnPs with characteristic folding and wrinkles due to the flexible nature of few-layered GnPs. As expected, the few-layered GnPs show typical SAED patterns of a six-fold symmetry with the {2110} spots appearing to be more intense relative to the {1100} spots (Figures S4a–S7a, insets), indicating also a high crystallinity.[23] Furthermore, the high-resolution TEM (HR-TEM) images display honeycomb-type morphologies for well-preserved basal planes (Figures S4d–S7d).

Elemental analysis (EA) data showed that the pristine graphite contains 99.64 wt % carbon with a negligible amount of oxygen (0.13 wt %), whereas the carbon content of EFGnPs was reduced to the range of 72.04–80.61 wt % (Table S1), presumably indicating the uptake of new elements at the edges of EFGnPs. Compared to the pristine graphite with undetectable hydrogen content, for example, the ball milling induced hydrogen in the HGnP was found to increase its weight by 2.98 wt %. The observed weight increase corresponds to the introduction of hydrogen per 2.3 carbon (C/H = 2.3) into the HGnP (Table S1), suggesting that the mechanochemically produced active carbon species can readily capture hydrogen to produce HGnP. Similarly, high oxygen and/or sulfur contents were found for CGnP (C/O = 3.4), SGnP (C/O = 11.4 and C/S = 21.8), and CSGnP (C/O = 8.1 and C/S = 69.4) (Table S1).

The FTIR spectrum of the pristine graphite shows only a weak band at 1632 cm^{-1}, which is characteristic of the vibration mode of adsorbed water molecules.[24] The strong peak at 3400 cm^{-1} is attributable to the bound moisture in KBr (Figure 2a), which was used for the preparation of the IR specimen. Due to

dx.doi.org/10.1021/ja3091643 | J. Am. Chem. Soc. 2013, 135, 1386–1393

the size reduction and hydrogenation at the edges, HGnP shows prominent peaks at 2850 and 2918 cm^{-1}, which are attributable to sp^3 C−H and sp^2 C−H, respectively, and in good agreement with EA (see Table S1). The CGnP and CSGnP display their characteristic peaks for carboxylic acid carbonyl (C═O) at around 1720 cm^{-1}, whereas the expected sulfonic acid sulfonyl (O═S═O) peaks at around 1360 cm^{-1} were not discernible for SGnP and CSGnP due to the strong inter- and intramolecular hydrogen bonding (Figure 2a), as reflected by the SEM morphologies (Figures 1e,f). The absence of IR signal from groups with strong hydrogen bonding has been observed for various materials.[25]

Along with the EDX (Figure 1g) and EA (Table S1) results, further evidence for the edge functionalization shown in Figure 1a comes from the XPS spectroscopic measurements. As can be seen in Figure 2b, the pristine graphite shows a strong C 1s peak at 284.3 eV with a very minor band at 532 eV due to physically adsorbed oxygen.[26,27] After the ball milling and subsequent exposure to air moisture, the EFGnPs show a significantly increased O 1s peaks relative to the corresponding C 1s peaks with increased C/O ratios in the range of 4.6−11.9 (Figures 2b and Table S2). The high-resolution XPS spectra for HGnP and CGnP, together with the curve fittings, show that the O element dominantly comes from O═*C*−*O*H (Figure S8). For SGnP and CSGnP, additional S 2p and S 2s peaks appeared at 164 and 228 eV, respectively (sky blue square box in Figure 2b), indicating the presence of sulfur-containing groups (e.g., $-SO_3H$) (Figure S9).

Thermogravimetric analysis (TGA) was used to quantitatively estimate the degree of functionalization. As shown in Figure 2c and Table S2, the pristine graphite displays a negligible amount of weight loss (0.3 wt %) up to 800 °C in nitrogen, whereas the corresponding weight losses for HGnP, CGnP, SGnP, and CSGnP are 82.2, 64.9, 86.8, and 82.0 wt %, respectively. The observed weight losses for EFGnPs were mainly caused by the thermal decomposition of edge groups via dehydrogenation (hydrogen), decarboxylation (carboxylic acid), and desulfonation (sulfonic acid) into hydrogen, carbon dioxide, and sulfur trioxide, respectively (see Figure S1).[16] Unlike the pristine graphite, all the EFGnPs exhibited gradual weight losses, suggesting the presence of strong intersheet interactions (e.g., H-bonding) between some of the polar edge groups to alter their decomposition behaviors.

The Raman spectra for the pristine graphite showed no detectable D band, while the G and 2D bands appeared at 1584 and 2970 cm^{-1}, respectively. Due to the large grain size (Figure 1b), the pristine graphite did not show a D band at around 1350 cm^{-1} associated with the edge distortions and topological defects. The ratio of the D- to G-band intensities (I_D/I_G) was zero. In contrast, all of the EFGnPs showed strong D bands around 1350 cm^{-1} (Figure 2d), and their I_D/I_G ratios were in the range of 0.79−1.50, indicating a significant size reduction by mechanochemical cracking and edge distortion by functionalization (see Figures 1a and S1). Interestingly, sulfonic acid containing SGnP and CSGnP displayed relatively sharper D and G bands than those of HGnP and CGnP, which was probably due to the formation of relatively bigger grain sizes and tighter aggregates by stronger surface interactions (H-bonding) between the sulfonic acids at their edges (see Figures 1d,e). In addition, SGnP and CSGnP showed the D′ band to the right shoulders of the G bands (arrows), which stems from another weak disorder on the graphitic structure associated with the strain induced by strong surface interactions.[21]

As shown in Figure 2e, the XRD diffraction pattern of the pristine graphite shows a typical strong [002] peak at 26.5°, which corresponds to an interlayer *d*-spacing of 0.34 nm, with all the other peaks attributable to other three-dimensional diffraction lines associated with hexagonal graphite (*h*-graphite).[22] In contrast, the corresponding XRD diffraction patterns for EFGnPs exhibit broad peaks over 15−30° with much weaker intensities, suggesting a high degree of exfoliation, even in the solid state. Unlike GO, which has a large shift of the [002] peak from 26.5° (*d*-spacing of 0.34 nm) to as low as 10.5° (*d*-spacing of 0.83 nm),[28] the EFGnPs show a significant decrease in intensities, while the peak location remains in the range of 22.3−25.9°, which corresponds to the interlayer *d*-spacing in the range of 0.40−0.34 nm (Figure 2f). These results implicate that the edges of EFGnPs are delaminated to a great extent without much lattice expansion. Hence, the ball-milling process involves not only mechanochemically cracking and edge-selectively functionalizing graphite but also delaminating graphite. The EFGnPs could be further exfoliated into few-layer GnPs upon dispersion in polar solvents (vide infra).

Hitherto, various structural characterization techniques have indicated that a large number of desired functional groups have been introduced at the broken edges of EFGnPs by ball milling of graphite in the presence of reactant gases and oxygenated groups by subsequent exposure to air moisture. The edge functionality (enthalpy gains) and size reduction (entropy gains) should provide thermodynamic driving forces for the dispersion of EFGnPs in various solvents. As a result, EFGnPs can disperse well in most protic and polar aprotic solvents, including neutral water (Figure S10a−d). Among all 16 tested solvents, polar aprotic solvents (e.g., DMAc, DMF, and NMP) were found to be good solvents for dispersing EFGnPs into stable dispersions with concentrations higher than 0.1 mg/mL. As expected, the polar nature of EFGnPs makes them less dispersible in nonpolar solvents, such as dichloromethane, toluene, and hexane.

In view of their high polarity, we further selected SGnP and CSGnP for ζ-potential measurements to ensure their dispersion stability at different concentrations in DMF as a basic solvent (Figure S10e,f). As indicated by the EA and XPS (Tables S1 and S2, respectively) studies, SGnP contained more sulfonic acid groups and hence more acidic in nature. As a result, SGnP displayed higher absolute values of the ζ-potential: −48.6 mV (0.04 mg/mL) and −38.8 mV (0.14 mg/mL) than the corresponding values for the CSGnP (−42.6 and −32.8 mV at 0.04 and 0.14 mg/mL, respectively) (Table S3). It is well-known that good dispersion stability via positive or negative charge repulsion can be achieved when the absolute value of ζ-potential is higher than 30 mV (Table S4).[27] Thus, the ζ-potential measurements, together with microscopic and spectroscopic studies (see Figures 1 and 2, respectively), indicate that the driving force for good dispersion stability must originate from the strong repulsion between the negatively charged $-SO_2-O^-$ generated in the basic DMF medium (vide infra).[29]

On the basis of TGA results, we heat-treated EFGnPs in a solid state at 900 °C under argon in order to thermally strip off the edge-functional groups into hydrogen, carbon dioxide, and sulfur trioxide and to restore the graphitic structures. Indeed, the resultant heat-treated EFGnPs (H-EFGnPs) showed much narrowed Raman D and G bands (Figure S11a) in comparison with those of starting EFGnPs (see Figure 2d). The XRD diffraction patterns also show that the interlayer *d*-spacing of H-

dx.doi.org/10.1021/ja3091643 | J. Am. Chem. Soc. 2013, 135, 1386−1393

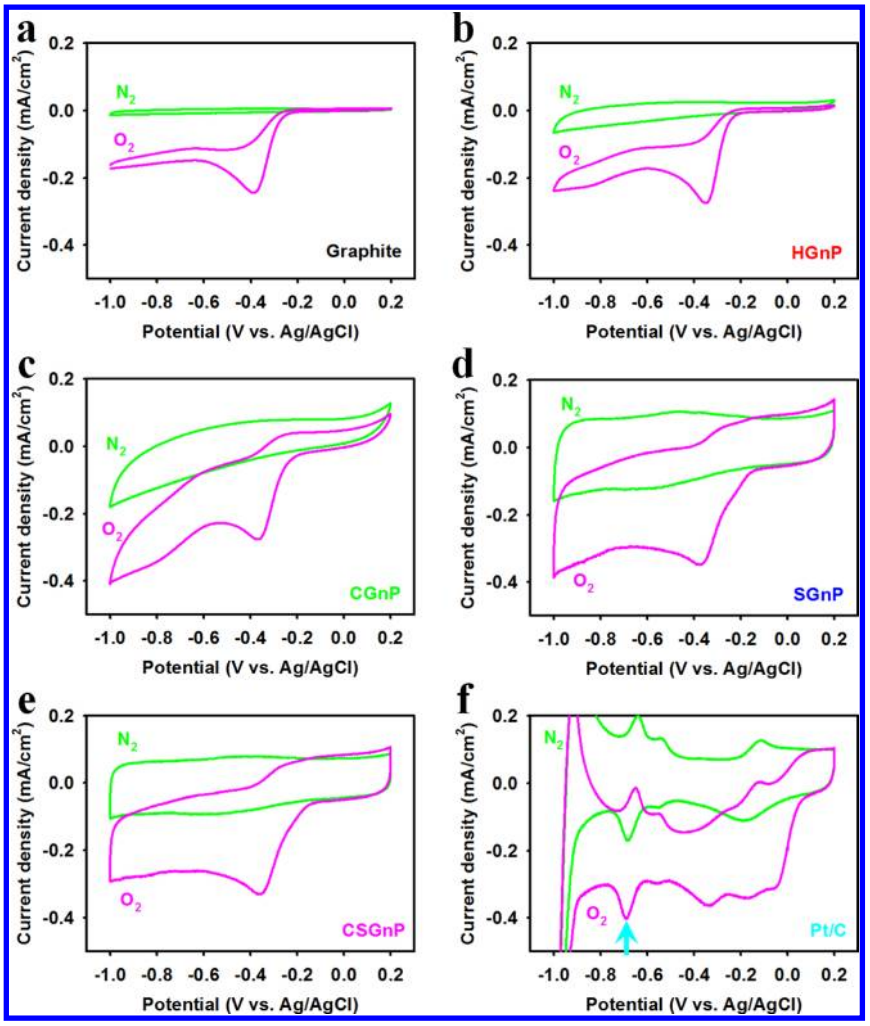

Figure 3. Cyclic voltammograms of sample electrodes on glassy carbon (GC) electrodes in N_2- and O_2-saturated 0.1 M aq KOH solution with a scan rate of 0.1 V/s: (a) pristine graphite; (b) HGnP; (c) CGnP; (d) SGnP; (e) CSGnP; and (f) Pt/C.

EFGnPs approaches 0.34 nm (Figure S11b), which is a typical interlayer distance of the pristine graphite (see Figure 2e). Thus, the graphitic interlayer *d*-spacing of H-EFGnPs has been largely restored by removal of the edge functional groups. Therefore, EFGnPs can be used as low-cost, stable precursors to high-quality graphene materials for many applications via simple solution processing, followed by thermal annealing, if necessary.

Finally, we evaluated the relationship between the electrocatalytic activity and edge polarity of EFGnPs for oxygen reduction reaction (ORR) in alkaline electrolyte. Because the polarities of edge groups are in the order of $-SO_3H$ > $-COOH$ > $-H$, the polarity order is expected to be SGnP > CSGnP > CGnP > HGnP > the pristine graphite. To start with, the polarities of EFGnPs were determined by contact angle measurements. The average contact angles (10 measurements) of SGnP, CSGnP, CGnP, and HGnP were 23.2, 34.3, 77.1 and 81.6°, respectively (Figure S12 and Table S5). As a result, a large number of sulfonic acids at the edges of SGnP and CSGnP were expected to be more hydrophilic for efficient oxygen absorption.[1] EFGnP electrodes were prepared by drop-coating each sample (0.5 mg) dispersed in Nafion/ethyl alcohol solution (1.5 mL) on a glassy carbon (GC) electrode. For comparison purposes, the pristine graphite and platinum (Pt) on activated carbon (Pt/C, Vulcan XC-72R) electrodes were also prepared by using the same procedure. Cyclovoltametric scans of EFGnPs show featureless voltammetric currents in N_2 saturated 0.1 M aq KOH solutions within the potential range of −1.0 to 0.2 V. As expected, the pristine graphite has the lowest capacitance, while the capacitances of EFGnPs increased in the order of HGnP < CGnP < CSGnP < SGnP (Figures 3b−e). Among all the tested samples, the SGnP showed the highest capacitance, which should correlate to its highest polarity rather than surface area (Table S6). The capacitance order was reproducible for five CV tests (Figure S13a) and linear sweep voltage (LSV) measurements (Figure S13b). All tested sample electrodes displayed a dramatic increase in voltametric currents in O_2 saturated solutions compared to the currents observed in the N_2 saturated electrolyte (Figure 3b−e). Hence, the high electrocatalytic activity of EFGnPs for ORR was evident. Specifically, the SGnP and CSGnP are much more efficient than the pristine graphite, HGnP and CGnP, in terms of low overpotential, high current density, and capacitance (Table S7). More specifically, the onset potentials of the sulfur-containing SGnP and CSGnP are similar at −0.16 V, and their maximum current densities are −0.38 and −0.28 mA/cm^2 at −1.0 V, respectively. The capacitances of SGnP (82.4 F/g) and CSGnP (69.7 F/g) are approximately 90 and 76% of the commercial Pt/C (91.9 F/g) in O_2 saturated 0.1 M aq KOH solutions (Table S5). However, considering the current contribution to

dx.doi.org/10.1021/ja3091643 | *J. Am. Chem. Soc.* 2013, 135, 1386−1393

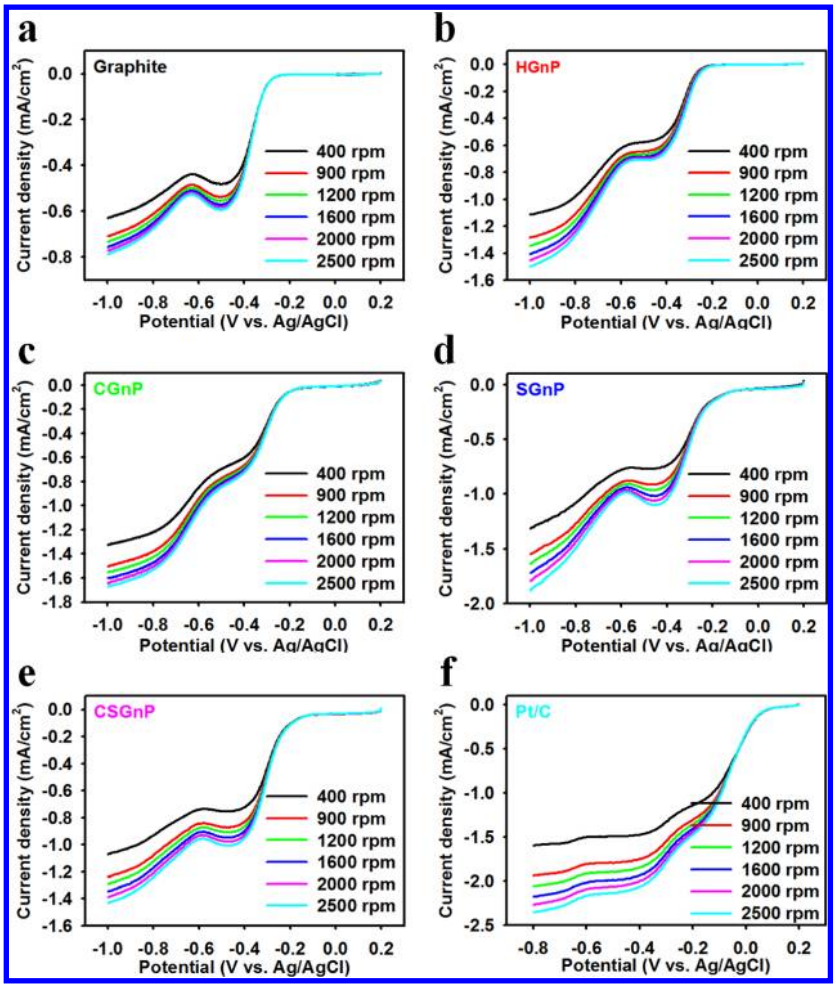

Figure 4. RDE voltammograms in O_2-saturated 0.1 M aq KOH solution with a scan rate of 0.1 V/s at different rotating rates of 400, 900, 1200, 1600, 2000, and 2500 rpm: (a) the pristine graphite; (b) HGnP; (c) CGnP; (d) SGnP; (e) CSGnP; and (f) Pt/C.

the reduction potential of hydrogen at around −0.7 V (sky blue arrow in Figure 3f), the pure ORR activities of SGnP and CSGnP are expected to be equivalent and/or even higher. The comparably high ORR activities of SGnP and CSGnP in alkaline condition are attributable to their acidic polar nature, and thus, strong polyelectrolyte effect in alkaline electrolyte stemming from sulfonic acids at their edges. The ionic interactions between strong acidic sulfonic acids on SGnP and CSGnP and strong basic KOH in the electrolyte solution make SGnP and CSGnP more hydrophilic. As a result, they have a strong affinity to electrolyte and oxygen. In conjunction to effective interactions with electrolyte, sulfonic acids at the edges of SGnP and CSGnP could be fully ionized in an alkaline medium to form a strong negative charge, as observed in ζ-potential measurements (Figure S10e,f).[30] As schematically presented for SGnP in Figure S13c, there must be strong charge repulsions between the graphitic layers in SGnP and CSGnP in alkaline electrolyte solutions to allow efficient oxygen diffusion into the graphitic layers for a more effective oxygen reduction. Compared with Pt/C, all EFGnPs displayed very good cycle stability in N_2-saturated electrolyte solutions (Figures S14a,b and S15). More importantly, SGnP and CSGnP displayed good cycle stability. They maintained 97.6 and 99.3% of initial capacitance after 100 cycles in O_2-saturated electrolyte solutions, while Pt/C showed only 88% (Figures S14c,d and S16). Thus, we believe both SGnP and CSGnP could be scalable as low-cost alternatives to expensive Pt-based electrocatalysts for ORR.

On the basis of a high current density and good cycle stability observed for SGnP and CSGnP, the reaction kinetics of EFGnP sample electrodes were studied by using a rotating disk electrode (RDE) (Figure 4). The oxygen reduction activities of the sulfur-containing SGnP and CSGnP (Figure 3d,e) are obviously more pronounced than those of the pristine graphite, HGnP, and CGnP (Figure 3a−c) and similar to that of commercial Pt/C (Figure 3f). In all cases, the voltammetric profiles showed that the current density was increased by increasing the rotating rate. Compared with the onset potentials of the pristine graphite (∼ −0.25 V) (Figure 4a), those of EFGnPs were gradually decreased according to their polarity order of HGnP (−0.24 V) < CGnP (−0.22 V) < CSGnP (−0.16 V) < SGnP (−0.16 V) (Figure 4b−e), though Figure 4a−e strongly suggested a two-electron ORR process at low potential. The corresponding Koutecky−Levich plots at the electrode potential ranges of −0.4 to ∼ −1.0 V revealed first-order reaction kinetics with respect to the concentration of dissolved O_2 (Figure S17).[31] As the detailed kinetic analysis described in the Experimental Section, the number of transferred electrons (n) involved in oxygen reduction can be analyzed on the basis of the Koutecky−Levich equation.[32] The n values for EFGnPs were increased from 2.2 to 3.8 as the applied voltage increased (Figure S17 and Table S8), indicating

dx.doi.org/10.1021/ja3091643 | J. Am. Chem. Soc. 2013, 135, 1386−1393

they are mainly two-electron transfer at low voltage and four-electron transfer at high voltage in the oxygen reduction process. The results are different from heteroatom-doped graphene[3,6] and commercial Pt/C.[2,4]

The overall electrocatalytic activities of EFGnPs are closely related to the edge polarity nature in the order of SGnP > CSGnP > CGnP > HGnP > the pristine graphite. In addition to the electron-accepting ability (thermodynamic contribution) of heteroatom-doped GnPs,[8] therefore, the oxygen diffusion kinetics could also significantly contribute to ORR. More importantly, both SGnP and CSGnP demonstrate comparable ORR activity at high potential (Figure S18) and superb cycle stability (Figure S14) to commercially available platinum-based electrocatalyst (Pt/C, Vulcan XC-72R, E-TEK).

■ CONCLUSIONS

We have developed a simple and versatile ball-milling process to efficiently exfoliate the pristine graphite directly into EFGnPs. Various microscopic and spectroscopic measurements were performed to confirm the reaction mechanisms for the edge functionalization of graphite by ball milling in the presence of reactant gases. The resultant EFGnPs are highly dispersible in various polar solvents suitable for simple solution processing. Compared to the less polar pristine graphite, HGnP and CGnP, more polar sulfur-containing SGnP and CSGnP, even without heteroatom doping in the graphitic carbon framework, displayed relatively high electrocatalytic activity and good cycle stability for ORR. In addition to the thermodynamic control of ORR via enhanced electron transfer induced by heteroatom doping into the graphitic basal plane, the kinetic contribution related to oxygen diffusion by edge polarity nature was demonstrated in this study to also play an important role in regulating the ORR process. The present work provides an important insight for designing a new class of carbon-based electrocatalysts. For example, heteroatom (thermodynamic contribution) doped GnPs with stable polar edge functional groups (kinetic contribution), such as sulfonic acid, would be expected to display maximum enhanced ORR activity. Hence, the ball-milling technique could be regarded as a powerful approach toward low-cost, high-yield production of EFGnPs with various functional groups of practical significance for the mass production of multifunctional materials and devices based on GnPs.

■ EXPERIMENTAL SECTION

Instrumentation. Fourier transform infrared (FTIR) spectra were recorded on Perkin-Elmer Spectrum 100 using KBr disks. TGA were conducted on a TA Q200 (TA Instrument) under nitrogen at a heating rate of 10 °C/min. The surface area was measured by nitrogen adsorption−desorption isotherms using the Brunauer−Emmett−Teller (BET) method on Micromeritics ASAP 2504N. The field emission scanning electron microscopy (FE-SEM) was performed on FEI Nanonova 230 while the HR-TEM employed in this work was a JEOL JEM-2100F (Cs) microscope operating at 200 kV. The TEM specimen was prepared by dipping carbon microgrids (Ted Pella Inc., 200 mesh copper grid) into well-dispersed samples in ethanol. XPS were recorded on a Thermo Fisher K-alpha XPS spectrometer. EA was conducted with Thermo Scientific Flash 2000, and ζ-potential values were determined using a Malvern Zetasizer (Nano ZS, Malvern Instruments). XRD patterns were recorded with a Rigaku D/MAZX 2500 V/PC with Cu−Kα radiation (35 kV, 20 mA, λ = 1.5418 Å). Raman spectra were taken with a He−Ne laser (532 nm) as the excitation source by using confocal Raman microscopy (Alpha 300S, WITec, Germany) in conjunction with atomic force microscopy (AFM). Contact angle measurements were conducted on a Krüss DSA 100 contact angle analyzer. Sample solutions were coated on a silicon (Si) wafer.

General Procedure for EFGnPs by Ball Milling Pristine Graphite in the Presence of Reactant Gases. In a typical experiment, the ball-milling graphite was carried out in a planetary ball-mill machine (Pulverisette 6, Fritsch) in the presence of hydrogen, dry ice (solid form of carbon dioxide), sulfur trioxide, or dry ice/sulfur trioxide mixture at 500 rpm. As a typical example, the pristine graphite (5.0 g, Alfa Aesar, natural graphite, 100 mesh (<150 μm), 99.9995% metals basis, lot no. 14735) and hydrogen (10 bar, Daesung Industrial Gases Co. LTD) for edge HGnP, dry ice (100 g, Hanyu Chemical Inc.) for edge CGnP, sulfur trioxide (7.0 g, Aldrich Chemical Inc.) for edge SGnP or dry ice/sulfur trioxide mixture for edge CSGnP were placed into a stainless steel capsule containing stainless steel balls of 5 mm in diameter. The container was fixed in the planetary ball-mill machine and agitated with 500 rpm for 48 h in all cases. Thereafter, the built-up internal pressure was very slowly released through a gas outlet. Upon opening the container lid in air at the end of ball milling, sparkling occurred in some cases due to the hydration by air moisture, as schematically shown in Figure S1. The resultant products were further Soxhlet extracted with a 1 M aqueous HCl solution to completely acidify the residual active species and to remove metallic impurities, if any. The final products were freeze dried at −120 °C under a reduced pressure (0.05 mmHg) for 48 h to yield 5.32 g of HGnP, 6.28 g of CGnP, 5.03 g of SGnP, and 5.23 g of CSGnP, respectively, as dark-black powder. Found for HGnP: C, 80.61%; H, 2.98%; N, 1.08%; O, 9.98%. Found for CGnP: C, 72.04%; H, 1.01%; O, 26.46%. Found for SGnP: C, 79.58%; H, 0.62%; O, 9.30%; S, 9.72%. Found for CSGnP: C, 79.49%; H, 0.83%; O, 13.11%; S, 3.66%.

■ ASSOCIATED CONTENT

Supporting Information

Detailed electrochemical measurements and characterization data from SEM, TEM, XPS, ζ-potential, Raman, contact angles, CV, LSV, electrochemical stability, Koutecky−Levich plot, EA, and BET. This material is available free of charge via the Internet at http://pubs.acs.org.

■ AUTHOR INFORMATION

Corresponding Author

jbbaek@unist.ac.kr

Author Contributions

[§]These authors contributed equally.

Notes

The authors declare no competing financial interest.

■ ACKNOWLEDGMENTS

This research was supported by WCU (World Class University), U.S.-Korea NBIT, Converging Research Center (CRC), Mid-Career and Basic Research Laboratory (BRL) programs through the National Research Foundation (NRF) of Korea funded by the Ministry of Education, Science. and Technology (MEST), and U.S. Air Force Office of Scientific Research through the Asian Office of Aerospace R&D (AFOSR-AOARD).

■ REFERENCES

(1) Yu, D.; Nagelli, E.; Du, F.; Dai, L. *J. Phys. Chem. Lett.* **2010**, *1*, 2165−2173.

(2) Lee, J. S.; Tai Kim, S.; Cao, R.; Choi, N. S.; Liu, M.; Lee, K. T.; Cho, J. *Adv. Energy Mater.* **2011**, *1*, 34−50.

(3) Qu, L.; Liu, Y.; Baek, J. B.; Dai, L. *ACS Nano* **2010**, *4*, 1321−1326.

(4) Li, X.; Wang, H.; Robinson, J. T.; Sanchez, H.; Diankov, G.; Dai, H. *J. Am. Chem. Soc.* **2009**, *131*, 15939−15944.

(5) Sheng, Z. H.; Gao, H. L.; Bao, W. J.; Wang, F. B.; Xia, X. H. *J. Mater. Chem.* **2011**, *22*, 390−395.
(6) Wang, S.; Zhang, L.; Xia, Z.; Roy, A.; Chang, D. W.; Baek, J. B.; Dai, L. *Angew. Chem., Int. Ed.* **2012**, *51*, 4209−4212.
(7) Jeon, I. Y.; Yu, D.; Bae, S. Y.; Choi, H. J.; Chang, D. W.; Dai, L.; Baek, J. B. *Chem. Mater.* **2011**, *23*, 3987−3992.
(8) Gong, K.; Du, F.; Xia, Z.; Durstock, M.; Dai, L. *Science* **2009**, *323*, 760−764.
(9) Niyogi, S.; Bekyarova, E.; Itkis, M. E.; McWilliams, J. L.; Hamon, M. A.; Haddon, R. C. *J. Am. Chem. Soc.* **2006**, *128*, 7720−7721.
(10) Li, D.; Müller, M. B.; Gilje, S.; Kaner, R. B.; Wallace, G. G. *Nat. Nanotechnol.* **2008**, *3*, 101−105.
(11) Xu, Y.; Bai, H.; Lu, G.; Li, C.; Shi, G. *J. Am. Chem. Soc.* **2008**, *130*, 5856−5857.
(12) Wang, X.; Li, X.; Zhang, L.; Yoon, Y.; Weber, P. K.; Wang, H.; Guo, J.; Dai, H. *Science* **2009**, *324*, 768−771.
(13) Hummers, W. S., Jr; Offeman, R. E. *J. Am. Chem. Soc.* **1958**, *80*, 1339−1339.
(14) Eda, G.; Fanchini, G.; Chhowalla, M. *Nat. Nanotechnol.* **2008**, *3*, 270−274.
(15) Park, S.; Ruoff, R. S. *Nat. Nanotechnol.* **2009**, *4*, 217−224.
(16) Stankovich, S.; Dikin, D. A.; Piner, R. D.; Kohlhaas, K. A.; Kleinhammes, A.; Jia, Y.; Wu, Y.; Nguyen, S. B. T.; Ruoff, R. S. *Carbon* **2007**, *45*, 1558−1565.
(17) Wang, X.; Zhi, L.; Müllen, K. *Nano Lett.* **2008**, *8*, 323−327.
(18) Boukhvalov, D. W.; Katsnelson, M. I. *J. Am. Chem. Soc.* **2008**, *130*, 10697−10701.
(19) Jeon, I. Y.; Shin, Y. R.; Sohn, G. J.; Choi, H. J.; Bae, S. Y.; Mahmood, J.; Jung, S. M.; Seo, J. M.; Kim, M. J.; Chang, D. W.; Dai, L.; Baek, J.-B. *Proc. Natl. Acad. Sci. U.S.A.* **2012**, *109*, 5588−5593.
(20) Sohn, G. J.; Choi, H. J.; Jeon, I. Y.; Chang, D. W.; Dai, L.; Baek, J. B. *ACS Nano* **2012**, *6*, 6345−6355.
(21) Liang, Y.; Wu, D.; Feng, X.; Müllen, K. *Adv. Mater.* **2009**, *21*, 1679−1683.
(22) Li, Z.; Lu, C.; Xia, Z.; Zhou, Y.; Luo, Z. *Carbon* **2007**, *45*, 1686−1695.
(23) Hernandez, Y.; Nicolosi, V.; Lotya, M.; Blighe, F. M.; Sun, Z.; De, S.; McGovern, I.; Holland, B.; Byrne, M.; Gun'Ko, Y. K. *Nat. Nanotechnol.* **2008**, *3*, 563−568.
(24) Stankovich, S.; Piner, R. D.; Nguyen, S. B. T.; Ruoff, R. S. *Carbon* **2006**, *44*, 3342−3347.
(25) Langner, R.; Zundel, G. *J. Phys. Chem.* **1995**, *99*, 12214−12219.
(26) Collins, P. G.; Bradley, K.; Ishigami, M.; Zettl, A. *Science* **2000**, *287*, 1801.
(27) Everett, D. H.; Chemistry, R. S. *Basic principles of colloid science*; Royal Society of Chemistry: London, 1988.
(28) Dikin, D. A.; Stankovich, S.; Zimney, E. J.; Piner, R. D.; Dommett, G. H. B.; Evmenenko, G.; Nguyen, S. B. T.; Ruoff, R. S. *Nature* **2007**, *448*, 457−460.
(29) Becerril, H. A.; Mao, J.; Liu, Z.; Stoltenberg, R. M.; Bao, Z.; Chen, Y. *ACS Nano* **2008**, *2*, 463−470.
(30) Kotin, L.; Nagasawa, M. *J. Am. Chem. Soc.* **1961**, *83*, 1026−1028.
(31) Allen, J. B.; Larry, R. F. Fundamentals and Applications. In *Electrochemical Methods*, 2nd ed.; Wiley: New York, 2001.
(32) Tammeveski, K.; Tenno, T.; Claret, J.; Ferrater, C. *Electrochim. Acta* **1997**, *42*, 893−897.